Nirwan Journal of Advanced Research (NJAR) **Article**
Vol. 01 | No. 01 | January- June 2026

Exploring Lead-Free Perovskite Alternatives: Comparative Analysis of $CH_3NH_3PbBr_3$ & $Cs_2AgBiBr_6$

Shaily Choudhary[1], Peeyush Kumar Kamlesh[2,*]
[1]Department of Physics, Quantum University, Roorkee, Uttarakhand (India)
[2]Department of Physics, Poornima University Jaipur, Rajasthan (India)
*Corresponding author: peeyush.physik@gmail.com

Abstract: *Double perovskites have emerged as a significant avenue for exploring diverse metals and oxidation states within halide perovskite compounds. Their remarkable properties and potential applications have captured increasing attention in recent times. These compounds, derived from the simple perovskite structure represented by the formula ABO_3, exhibit a wide range of intriguing characteristics. The perovskite structure's flexibility in both composition and structure allows for the incorporation of nearly all elements from the periodic table. Researchers have delved into the structural, electronic, and optical properties of double perovskite $Cs_2AgBiBr_6$ using first principles methods, comparing them with those of hybrid perovskites like $CH_3NH_3PbBr_3$.*

[Key Words: *Double Perovskite, First-Principles Method, Hybrid Perovskites, Electronic Properties, Optical Properties****]***

1. Introduction:

Solar power stands out as one of the most abundant energy sources available globally. The sheer magnitude of sunlight's energy potential is staggering, with a year's worth containing approximately 1.5×10^{18} kWh of energy. In stark comparison, the combined known reserves of oil, coal, and gas amount to only 1.75×10^{15} kWh, 1.4×10^{15} kWh, and 5.5×10^{15} kWh, respectively (Sum et al. 2014). This vast difference underscores the immense potential of solar energy, offering over a hundred times more energy than the world's entire known fossil fuel reserves combined. The challenge has always been efficiently and economically harnessing this abundant resource. Photovoltaic cells have emerged as a promising solution, directly converting sunlight into electricity. To make solar energy competitive with fossil fuels and secure a significant portion of the electricity market, it's imperative to reduce the overall cost of solar energy. This can be achieved by either lowering the cost of photovoltaic cells or increasing their power conversion efficiency. Among the most notable developments in this field are solar cell materials based on organo-lead halide perovskites. These materials have garnered significant attention due to their rapidly increasing solar-to-electricity conversion efficiencies. Additionally, their ease of solution-based processing at low temperatures and strong optical absorption properties make them attractive candidates for solar energy applications, despite concerns regarding their stability (Eames et al. 2015).

In 2012, a significant advancement in hybrid perovskite photovoltaic (HPPV) architecture emerged when researchers replaced the liquid electrolyte with solid-state hole-transporting materials, achieving a noteworthy 10% power conversion efficiency (PCE). This breakthrough sparked a rapid improvement in PCE, leading to the current record of HPPVs surpassing the 20% mark. Hybrid perovskites, serving as photoactive materials, offer several key advantages in photovoltaic applications. These include band gaps that closely align with the optimal values for single-junction solar-cell absorbers, exceptional light absorption properties within the visible spectrum of sunlight, and high electron and hole transport mobilities. Furthermore, their attributes such as low-temperature processing, cost-effectiveness, lightweight nature, and environmental friendliness make them attractive options for solar-cell devices, promising clean, affordable, and sustainable energy solutions (Li et al. 2016). However, despite their potential, HPPVs suffer from certain drawbacks, notably instability and susceptibility to moisture, heat, and prolonged light

exposure, as well as concerns about toxicity due to the presence of lead (Pb) (Jung et al.2015, Slavney et al. 2017).

Although lead halide perovskites exhibit exceptional optoelectronic properties, concerns regarding their stability and toxicity pose significant barriers to their commercialization in device applications. These materials have demonstrated sensitivity to moisture and light exposure, despite considerable progress in addressing these issues. However, the long-term stability of lead halide perovskites and their devices remains a substantial concern within the scientific community. Additionally, the presence of lead, known for its high bioavailability in these materials, raises contentious debates in the field. Consequently, since the early stages of perovskite research, there has been a notable interest in exploring alternative materials that offer improved environmental friendliness and stability.In pursuit of more sustainable options, two primary strategies have emerged to mitigate the toxicity and stability challenges associated with lead halide perovskites. Firstly, researchers have investigated substituting lead with elements that are less harmful. For instance, homovalent substitutions involving metals like Sn^{II} or Ge^{II} have been explored to produce perovskite compositions with the general formula $AB^{II}X_3$, where A represents a monocation (e.g., Cs, methylammonium (MA), or formamidinium (FA)) and X denotes a halide (Cl, Br, or I). Substituting lead with these metals, particularly tin, has led to the development of solar cells with respectable efficiencies of up to 13.2% (Vargas et al. 2020).

In recent years, double perovskite compounds have garnered growing interest because of their intriguing properties and potential applications. These compounds are derived from the simple perovskite structure, which has a general formula of ABO_3 and is renowned for its diverse range of properties. The structural and compositional flexibility of perovskite materials allows them to accommodate nearly all elements of the periodic table (Dasgupta et al. 2020).

Through extensive research, scientists have investigated a wide array of material combinations, ultimately identifying perovskites containing lead (Pb), tin (Sn), and germanium (Ge) as having significant potential for optoelectronic devices. Additionally, endeavours have been undertaken to explore structures akin to perovskites through double perovskites. In these structures, the substitution of two neighbouring divalent lead cations with monovalent and trivalent ions has been explored, offering a pathway to expand the scope of materials with desirable properties (Giustino et al. 2016). Double perovskites, a broad category of condensed materials, have been under investigation since the 1960s (Cheng et al. 2006, Wu et al.2001). They represent one of the most extensively studied compound families due to their structurally flexible nature, which enables innovative device applications stemming from their low reactivity, as well as their magnetic and optical properties (Shimakawa et al. 2011). Double perovskite oxides, denoted as $AA'BB'O_6$, where A represents an alkaline-earth or rare-earth metal, and B and B′ denote transition metals, are derived from the simple ABO_3 perovskite structure. In these specific structures, the A-site atoms are typically comprised of alkaline earth metals such as Barium (Ba), Strontium (Sr), or lanthanides, whereas the B atoms denote transition metals. This category of materials constitutes a significant class characterized by structural deviations from the cubic space group Fm3m (No. 225) structure. This research aims to enhance the comprehension of the double perovskite $Cs_2AgBiBr_6$ by conducting an in-depth analysis of its electronic and optical properties. Utilizing the first principles method within the density functional theory (DFT) framework with the Perdew-Burke-Ernzerhof (PBE) exchange-correlation functional, this study employs the full potential linearized augmented plane wave (FPLAPW) method. The investigations are carried out using the WIEN2k code (Tran et al. 2018). a computational tool grounded in the density functional theory (DFT) framework, facilitating a meticulous examination of the material's electronic and optical characteristics (Hohenberg et al. 1964).

Typically, the general formula for the perovskite structure is ABO_3, which shares the same crystal structure as $CaTiO_3$ for this class of compounds. The structure of perovskite was initially described by Victor Goldschmidt in 1926, and he focused on tolerance factors (Johnsson et al. 2005). The Goldschmidt Tolerance Factor (t) is a widely used geometric ratio for the perovskite structure (Li et al. 2016, Luo et al. 2015), where it represents the ratio of the distance A-X to the distance B-X in an idealized solid-sphere model. It is denoted by 't' and formulated as (Green et al. 2014, Bartel et al. 2019).

$$t = (rA + rX)/\{\sqrt{2(rB + rX)}\}$$

Where, the ionic radius of the A and B cations is represented by r_A and r_B respectively, while the ionic radius of the anion is denoted by r_X. The ability of the A cation to fit within the cavities in the BX_3 framework is determined by the tolerance factor.

This investigation will concentrate on the advancements in perovskite and double perovskite, along with their characteristics, electronic, and optical structures. Initially, the intrinsic physical and electronic properties of $CH_3NH_3PbBr_3$ and $Cs_2AgBiBr_6$ were examined, followed by a comparison of their structural, electronic, and optical properties.

2. Computational Details:

This study employed first-principlesinvestigations based on the Kohn-Sham DFT framework to explore the structural, electronic, and optical characteristics of the lead-free halide double perovskite $Cs_2AgBiBr_6$. The computations were carried out using the WIEN2k code, incorporating principles from previous studies (Tran et al. 2018, Choudhary et al. 2020, Kohn et al. 1965). In order to attain optimized lattice constants and ground state energy for the lead-free halide double perovskite, structural calculations were carried out, enabling the system to adequately relax within the cubic phase. This relaxation process was facilitated using the Wu-Cohen generalized gradient approximation (WC-GGA), which allowed for the determination of optimized lattice constants. Furthermore, the Perdew-Burke-Ernzerhof (PBE) generalized gradient approximation (GGA) exchange-correlation functional was applied to ensure accurate calculations and reliable results (Perdew et al 1996). To ensure a well-converged self-consistent field (SCF) calculation, parameters such as a cutoff energy of -6.0 Ry, $R_{MT} \times K_{max}$ = 7, and 125 k-points, which generated a 5×5×5 k-mesh in the first Brillouin zone, were utilized (Monkhorst et al. 1976). All computations were conducted using the full potential linearized augmented plane wave (FP-LAPW) method within the DFT framework as implemented in the WIEN2k code.The optical properties were evaluated for a dense unit cell with 10,000 k-mesh points. It's important to note that all predictions were based on 0 K DFT-relaxed structures and did not consider lattice expansion or temperature-induced phase changes.

3. Results and Discussion:

3.1. Structural Properties:

Optimizing material structure parameters is essential for understanding the structural behavior of materials under different temperatures and pressures. Ground-state properties such as lattice constant (a), unit cell volume (V0), bulk modulus (B), and its pressure derivatives (B') are evaluated through the volume optimization process. The structural characteristics of $CH_3NH_3PbBr_3$, as investigated in a prior study, are depicted in Figure 1 (Choudhary et al. 2020).

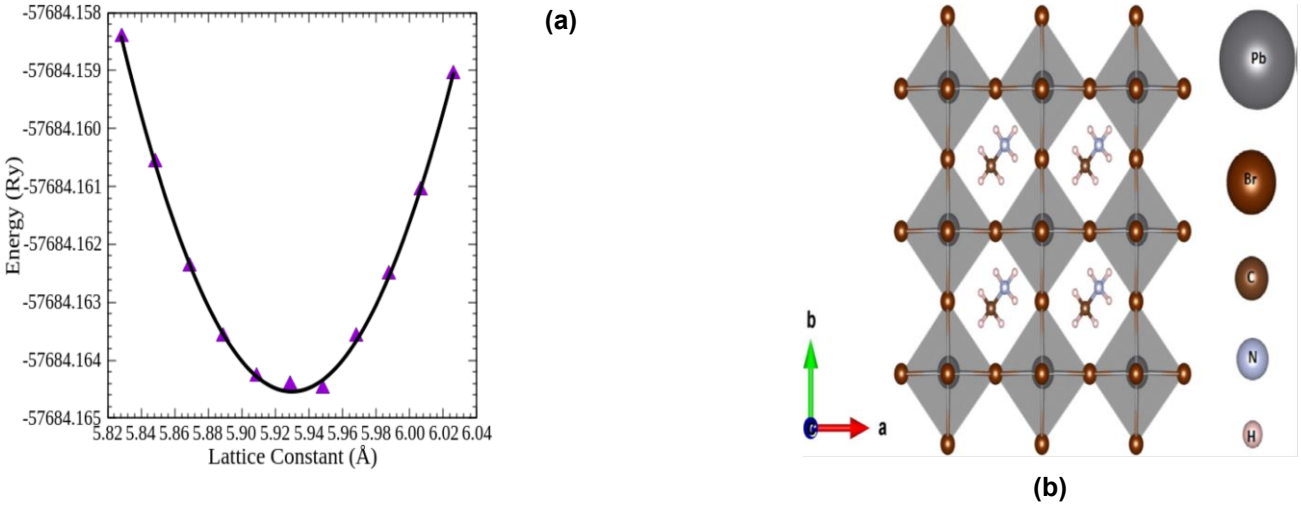

Figure 1: (a) Calculated total energy vs lattice constant cubic $CH_3NH_3PbBr_3$ using WC-GGA potential. **(b)** The schematic optimized structure of $CH_3NH_3PbBr_3$ perovskites (Choudhary et al. 2020).

This study involves the optimization of the structure of $Cs_2AgBiBr_6$, employing the Perdew-Burke Ernzerhof Generalized-Gradient Approximation (PBE-GGA) method to accurately consider the exchange correlation effect. The determination of ground state structural properties, such as equilibrium volume (V_o), bulk modulus (B_o), pressure derivative of bulk modulus (B_o'), and ground state energy (E_o), is accomplished by fitting the total energy against the reduced and extended volume of the unit cell to the third-order Birch-Murnaghan equation of state (EOS) (Birch et al. 1947].

$$E(V)=E_o+\frac{9V_oB_o}{16}\left\{\left[\left(\frac{V_o}{V}\right)^{2/3}-1\right]^3 B'_o+\left[\left(\frac{V_o}{V}\right)^{2/3}-1\right]^2 x\left[6-4\left(\frac{V_o}{V}\right)^{2/3}\right]\right\}$$

Where, E_o represents the total energy, V_o denotes the equilibrium volume, B_o represents the bulk modulus at pressure p=0, and B_o' represents the first derivative of bulk modulus with respect to pressure. This approach ensures a comprehensive understanding of the material's structural characteristics and its behaviour under different conditions.The energy versus volume curve for $Cs_2AgBiBr_6$, obtained through geometry optimization, is depicted in Figure 2, showcasing lattice parameters (a_o), equilibrium volume (V_o), bulk modulus (B), and pressure derivative of bulk modulus (B_o') for GGA-PBE potentials, respectively.The shape of energy vs volume curve shows good, relaxed optimization of $Cs_2AgBiBr_6$ (figure 2). The value of lattice constant (a_0) is investigated to be 13.75 Å. The relationship between energy and volume of unit cell helps us to calculate the lowest internal energy of unit cell.

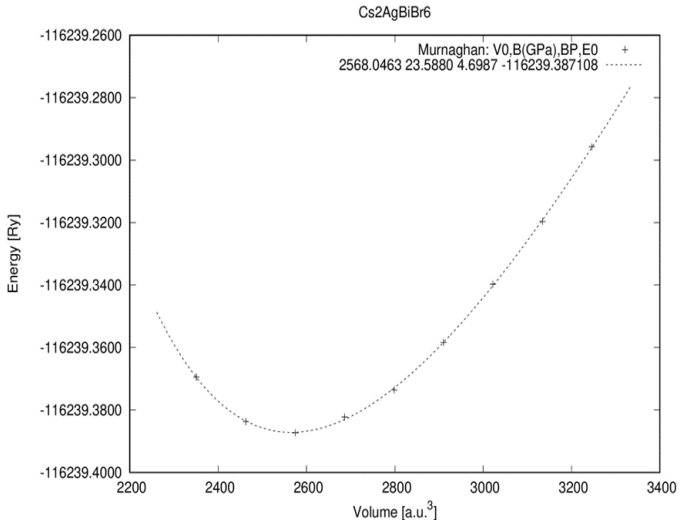

Figure 2 - Calculated total energy versus the lattice constant for cubic double Perovskites $Cs_2AgBiBr_6$ using GGA-PBE Calculation without SOC calculations.

3.2. Electronic Properties:

In order to gain insights into the band gap properties and elucidate the contributions of orbital electrons and atoms to the maximum of the valence band and minimum of the

conduction band, a thorough analysis of both the band structure and density of states is imperative. Figure 3(A) in this study presents the electronic band structure alongside the total density of states of $CH_3NH_3PbBr_3$, offering a comprehensive view of the distribution of electronic states within the material. Furthermore, Figure 3(B) offers insights into the partial density of states (PDOS) originating from different orbital components of key elements such as Pb, Br, and CH_3NH_3, providing a detailed understanding of their individual contributions to the electronic structure of the compound. Through these analyses, researchers can effectively discern the fundamental electronic properties and orbital characteristics that govern the behaviour of the material, facilitating the further exploration of its potential applications in optoelectronic devices.

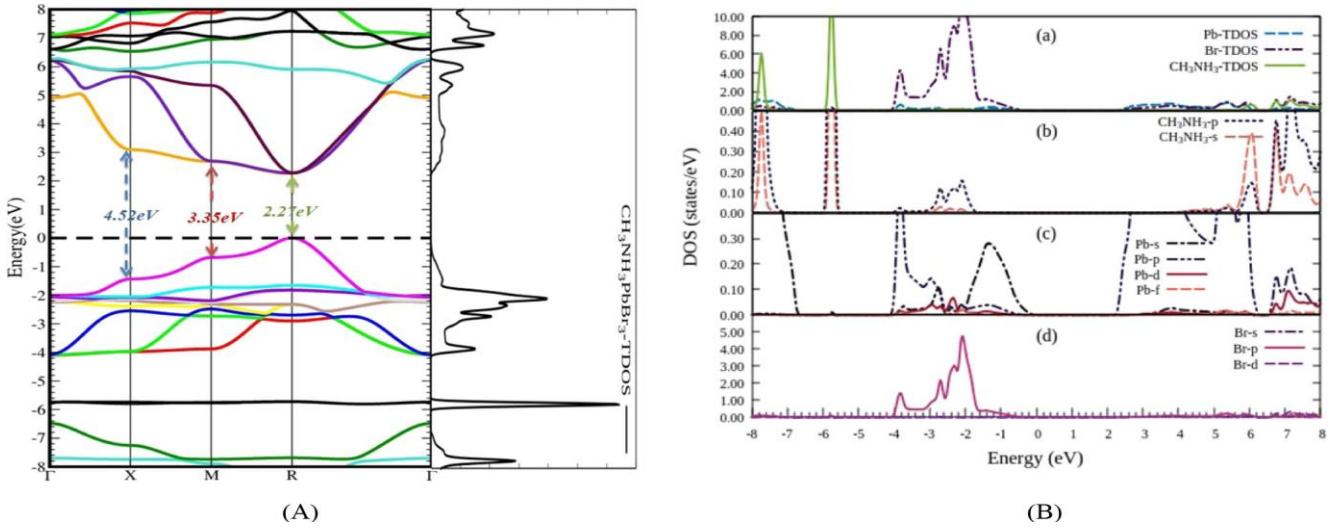

Figure 3: (A) Band structure and **(B)** Partial density of state for $CH_3NH_3PbBr_3$, where zero energy corresponds to the Fermi level ((Choudhary et al. 2020).

As highlighted in earlier research, it has been established that the valence band maximum (VBM) primarily consists of an antibonding combination of 6s orbitals from lead (Pb) and 4p orbitals from bromine (Br). These orbitals contribute significantly to the electronic structure near the top of the valence band, influencing the material's properties. Conversely, the conduction band minimum (CBM) predominantly comprises Pb 6p orbitals and bromine 4s orbitals, which define the energy levels near the bottom of the conduction band, impacting the material's conductivity and optical properties.Moreover, the presence of methylammonium ions near the Fermi level has been found to have minimal impact. Their filled states reside well below the VBM, indicating limited involvement in the electronic properties around the Fermi level. Similarly, their empty states are positioned above the CBM, suggesting minimal influence on the electronic structure near the bottom of the conduction band (Choudhary et al. 2020).

Understanding these contributions aids in deciphering the electronic behaviour of the material and its suitability for various applications in optoelectronics.

In order to characterize the atomic orbitals in the electronic band structure and partial density of states (PDOS) were calculated. Meanwhile, we have studied the charge density distribution of the main structure, particularly the conduction band (CB) and the valance band (VB). Thus, according to plotted band structure curve and the coordinate of the k points figure 4(a), it is clear that this is a semiconductor with an indirect band gap. The calculated band gap for $Cs_2AgBiBr_6$ along the high symmetric point of Brillion zone is 1.8 eV with the GGA–PBE (without SOC) exchange-correlation potential.

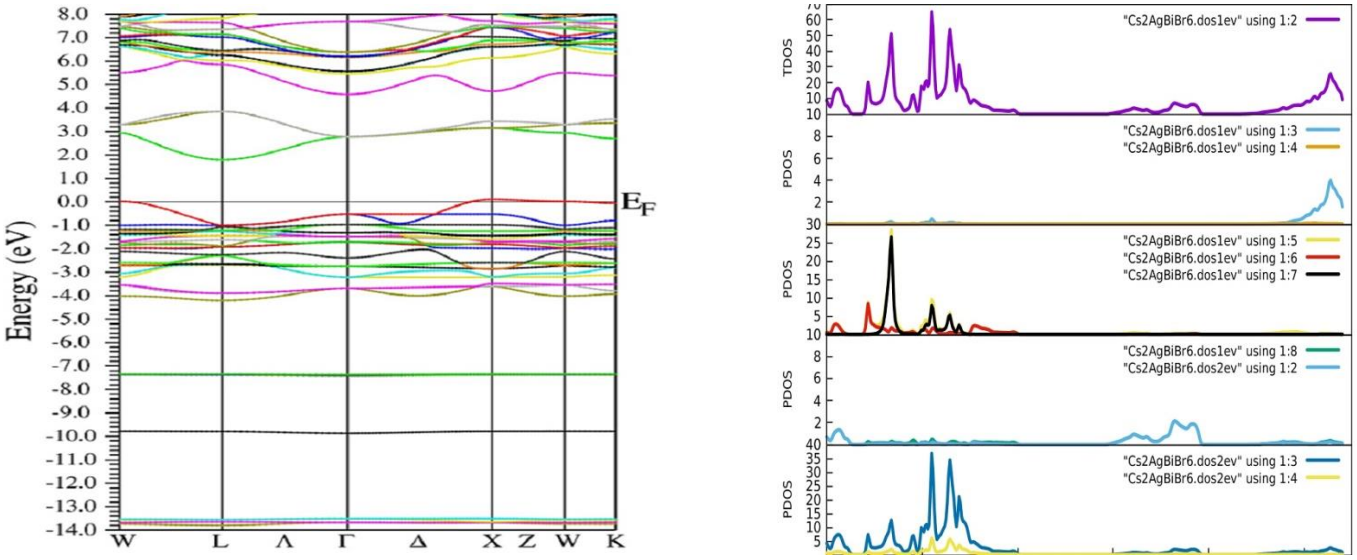

(a) (b)

Figure 4: (a) Energy band structure of $Cs_2AgBiBr_6$ using GGA-PBE Calculation without SOC calculations. **(b)** Total and Partial density of state (TDOS & PDOS) of $Cs_2AgBiBr_6$, where zero energy corresponds to the Fermi level.

The total and partial density of states calculations, using GGA-PBE approximations for $Cs_2AgBiBr_6$ in cubic lead-free halide double Perovskites structure are shown in Figure 4(b), in which, Fermi energy is selected as zero reference point. By comparing the TDOS and PDOS plot with the band structure a good adaptation has been seen. Total density of states can be explained by dividing the curve into three regions. The valence to conduction band transition is primarily from filled halogen 3p/4p states to anti bonding Ag 5s and Bi 6p states. This can be seen by looking at the partial density of state diagrams (PDOS) in figure 6. The participation of both Ag and Bi orbitals to the lower energy conduction bands is key to maintaining some dispersion of the conduction band. Although the valence band is largely halogen 3p/4p in character, there is extensive admixture of Ag 4d states, which results in the presence of several relatively flat bands. The presence of Ag 4d states plays a role in reducing the band gap.

3.3. Optical Properties:

The dielectric properties play a crucial role in providing understanding into the optical characteristics and possible applications of a material. The macroscopic optical response of a compound is described by its dielectric function within the realm of linear response. This dielectric function is primarily associated with the electronic response (Ece et al. 2010).

To investigate the optical absorption characteristics of the lead-free halide double perovskite $Cs_2AgBiBr_6$, it is essential to introduce the complex dielectric function. It is commonly understood that the complex dielectric function varies with frequency, and its imaginary part can be expressed as follows:

$$\varepsilon_1(\hbar\omega) = \frac{2e^2\Pi}{\Omega\varepsilon_0}\sum_{c,v,k}|\langle\varphi_k^c|\hat{u}.r|\varphi_k^v\rangle|^2\delta\, E_k^c E_k^v\,(\hbar\omega)$$

The parameters are defined as follows: φ_k^c and φ_k^v represent the wave functions of the unoccupied state and occupied state at the k-point reciprocal space, respectively. The symbol ˆu denotes the polarization vector for the incident electronic field. Other symbols such as u, U, and r refer to the photon frequency, cell volume, and momentum operator, respectively.

The real part of the complex dielectric function can be easily derived using the well-known Kramers–Kronig relationship:

$$\varepsilon_1(\omega) = 1 + \frac{2}{\pi}\,P\int_0^\infty \frac{\omega'\varepsilon_2(\omega')}{\omega'^2-\omega^2}\,d\omega'$$

Where P refers to the principal value of the integral.

The imaginary part, $\varepsilon_2(\omega)$ indicates the optical absorption transitions in the material and is closely linked to the band structure (Ziati et al. 2021). The frequency-dependent equation for $\varepsilon_2(\omega)$ is:

$$\varepsilon_2(\omega) = \frac{8}{2\pi\omega^2}\sum |P_n(x)|^2 \frac{dS_x}{\nabla\omega_n(k)}$$

Here, $P_n(x)$ denotes the dipole momentum matrix for the external band transformation.The imaginary and the real parts of dielectric spectra are indicated in Figure5(a) and 5(b) respectively.

The real part of dielectric function $\varepsilon_1(\omega)$ displayed in figure5(b) giving the information about the polarizability of a material, the obtained static dielectric constant is $\varepsilon_1 = 4.2$ at zero. It starts increasing from zero frequency limit and reach the maximum value of 7.6 at 2.8eV and goes 0.5 for the ranges 3.9 to 4.2 eV. In these graphs xx, yy and zz axis overlap each-other and xy, yz and xz axis doesn't take any contribution in the spectrum.

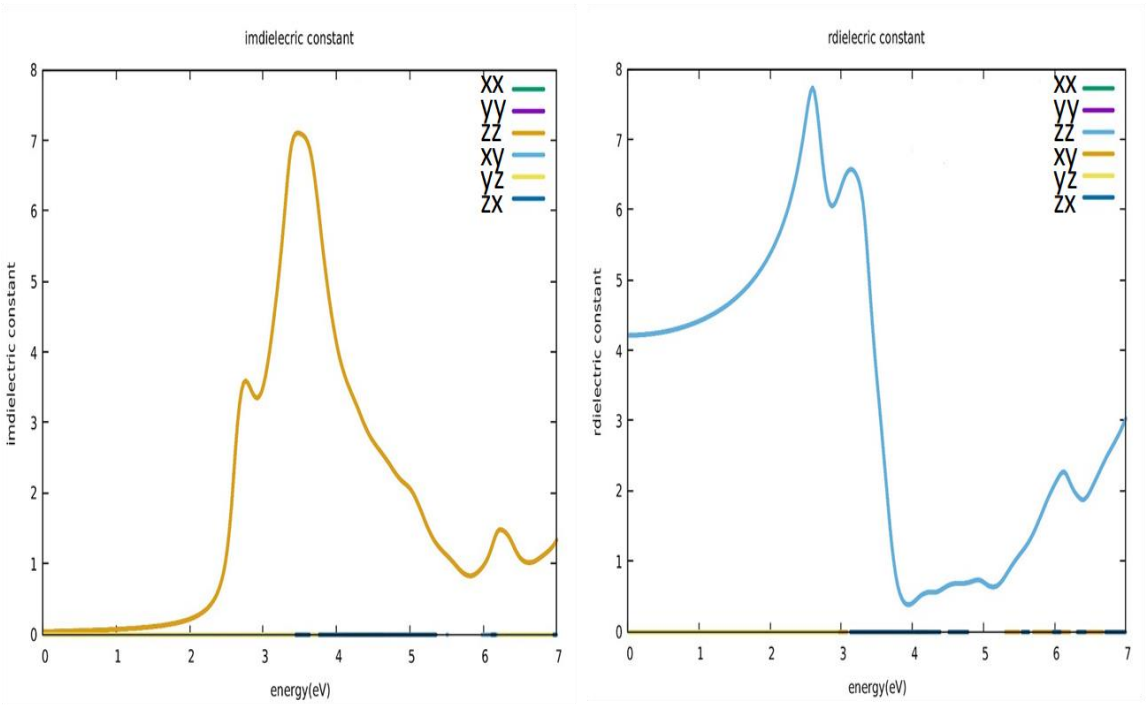

Figure 5: Spectra of optical properties as a function of photon energy for lead free halide double perovskite $Cs_2AgBiBr_6$, **(a)**Imaginary part $\varepsilon_2(\omega)$ and **(b)** real part $\varepsilon_1(\omega)$ of dielectric function.

The frequency-dependent optical absorption coefficient can be derived from the following equation:

$$\alpha(\omega) = \sqrt{2}\,\omega\sqrt{-\varepsilon_1(\omega) + \sqrt{\varepsilon_1^2(\omega) + \varepsilon_2^2(\omega)}}$$

To prove optical harvesting capability, we next examined other optical parameters for the investigated $Cs_2AgBiBr_6$ double perovskite material.The information of absorption nature of $Cs_2AgBiBr_6$ can be extracted from imaginary part $\varepsilon_2(\omega)$.

The critical energy point of the dielectric function is identified at E_0 = 2.34 eV, aligning with the direct band gap at equilibrium conditions. This indicates a significant optical transition occurring at this energy level, influencing the material's absorption characteristics. Upon examination of figure 6(a), it is evident that there exists a pronounced absorption peak within the energy range of 2.3-6.6 eV for the imaginary part $\varepsilon_2(\omega)$ of the dielectric function. This peak signifies the energy range over which the material exhibits strong absorption of incident light, suggesting its potential suitability for optoelectronic applications within this spectral range. The prominent peak observed at 3.6 eV represents the peak absorption within the material. It indicates the energy level at which the material exhibits the highest

absorption of incident light, suggesting its strong interaction with electromagnetic radiation at this specific energy. This peak is crucial for understanding the material's optical behavior and its potential applications in photonic devices.

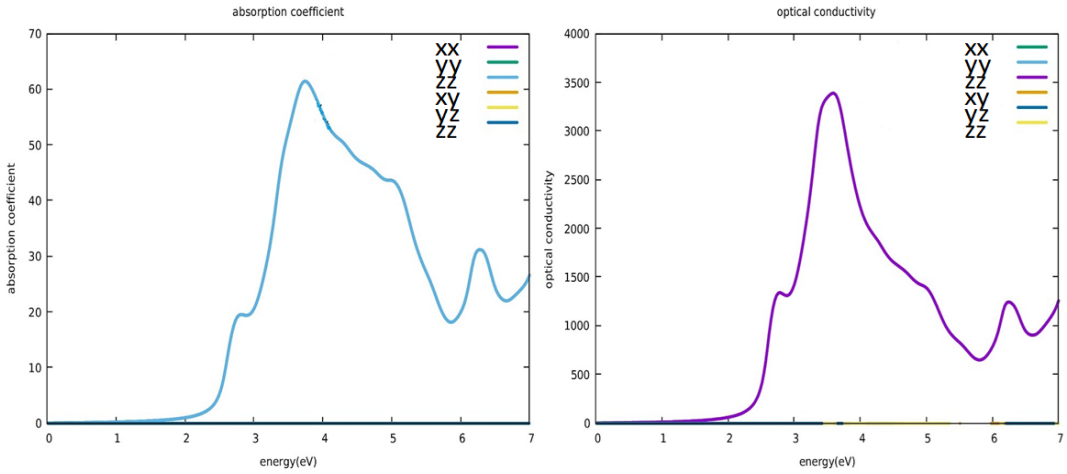

Figure 6: (a) Absorption coefficient α(ω) and **(b)** Optical conductivity σ(ω).

Figure 6(b) illustrates the optical conductivity (σ(ω)) of the material, beginning from 1.8 eV. The optical conductivity quantifies the material's ability to conduct electricity under the influence of light. It is noteworthy that the maximum value of optical conductivity occurs at 3.5 eV. This indicates that the material exhibits its highest conductivity at this energy level, reflecting its efficient response to electromagnetic radiation within this spectral range.

Corresponding features are also determined in absorption coefficient α(ω) in the absorption range up to 7 eV shown in figure 6(a). The basic understanding of the material is provided by absorption spectra and electronic structure. The absorption spectra and the imaginary part of dielectric function $\varepsilon_2(\omega)$ are directly proportional of each other. The maximum absorption occurs at 3.7 eV. Like previous graphs, in these graphs xx, yy and zz axis overlap each-other and xy, yz and xz axis also doesn't take any contribution in the spectrum.

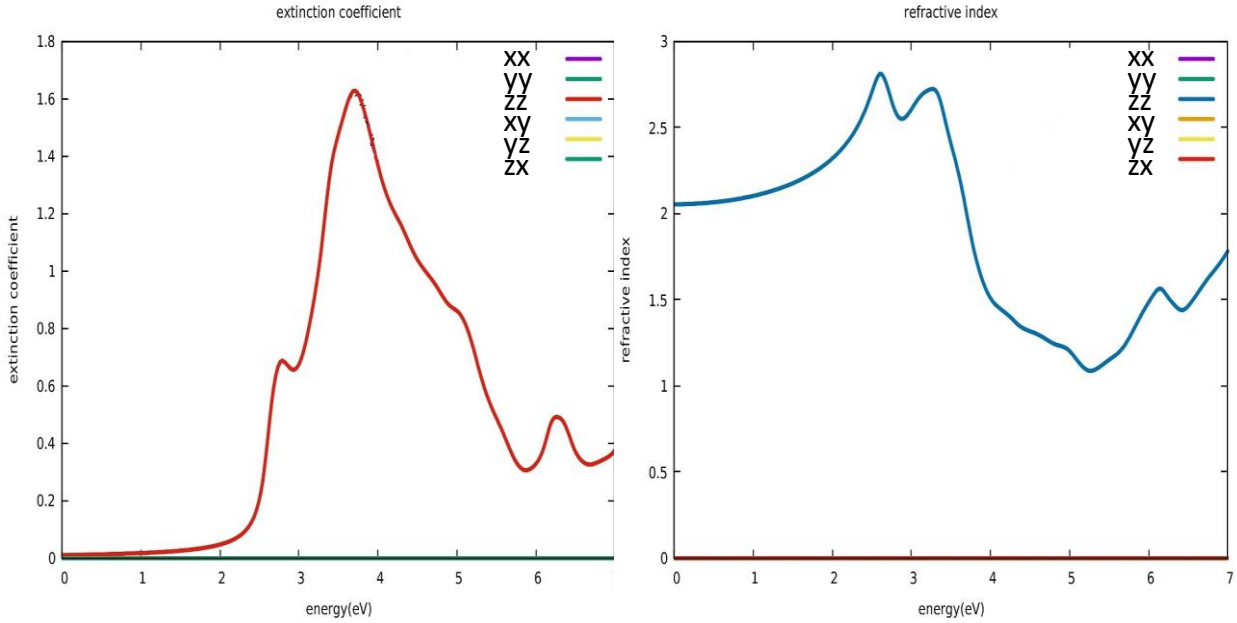

Figure7: (a) Extinction coefficient k(ω) and **(b)** Refractive index n(ω).

In figure 7(a) and 7(b) the extinction coefficient and refractive index are displayed; from figure we can observe the optically isotropic nature of lead-free halide double perovskite $Cs_2AgBiBr_6$ in the lower energy range.The value of refractive index for lower energies is almost constant but it attains the maximum value as the energy increases. The value of refractive index n(0) is 2.1. It gains a peak in the U.V. range at 2.5eV. The value of refractive index n(0) > 1 because of the photons interaction with electrons. Essentially, any mechanism that augments the density of electrons in a material also elevates the refractive index of that material. This relationship underscores the influence of electron density on the optical properties of a substance, particularly its ability to interact with and bend light as it passes through.

The behaviour of imaginary part of dielectric function $\varepsilon_2(\omega)$ and extinction coefficient $k(\omega)$ shows a similar trend that can be observed from figures 5(a) and 7(a) and 3.8 eV is the maximum absorption in the medium of extinction coefficient $k(\omega)$.Like previous graphs, in these graphs also xx, yy and zz axis overlap each-other and xy, yz and xz axis also doesn't take any contribution in the spectrum. The optical reflectivity $R(\omega)$ is displayed in figure 8. The point where the maximum reflectivity occurs and the point where real part of dielectric function goes below zero is very near about. The maximum value of reflectivity is at 3.8 eV. Also here, xx, yy and zz axis again overlap each-other and xy, yz and zx doesn't take any contribution in the spectrum.Understanding the optical conductivity profile is essential for assessing the material's suitability for various optoelectronic applications, including solar cells, photodetectors, and light-emitting diodes.

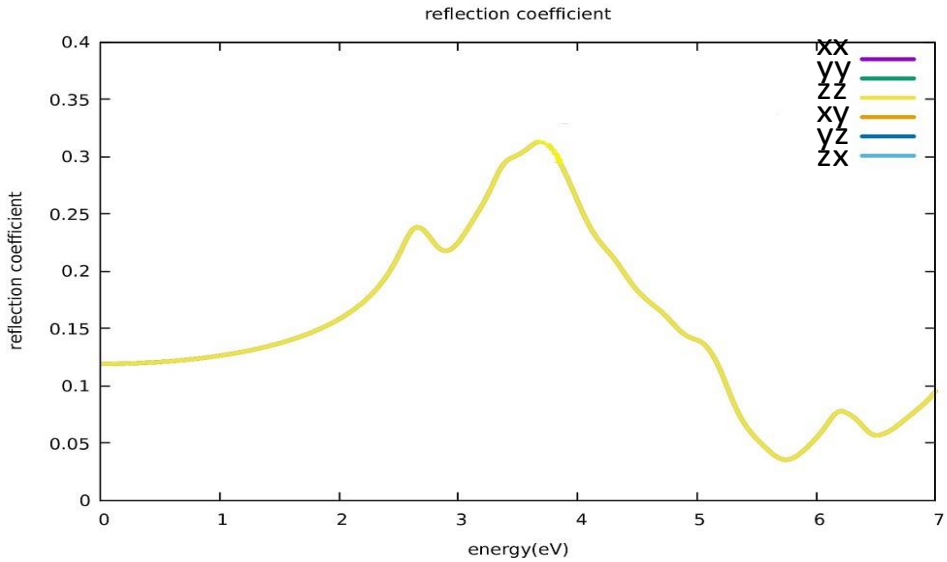

Figure 8: Reflectivity R(ω).

For the purpose of comparison, the optical properties of $CH_3NH_3PbBr_3$, which were previously computed in our study, are presented in figures 9 and 10. These figures provide insights into the optical behaviour of $CH_3NH_3PbBr_3$, allowing for a comparative analysis with the optical properties of the current material under investigation. By juxtaposing the optical characteristics of both materials, researchers can gain a deeper understanding of their respective optical responses and identify potential similarities or differences that may impact their performance in optoelectronic applications.

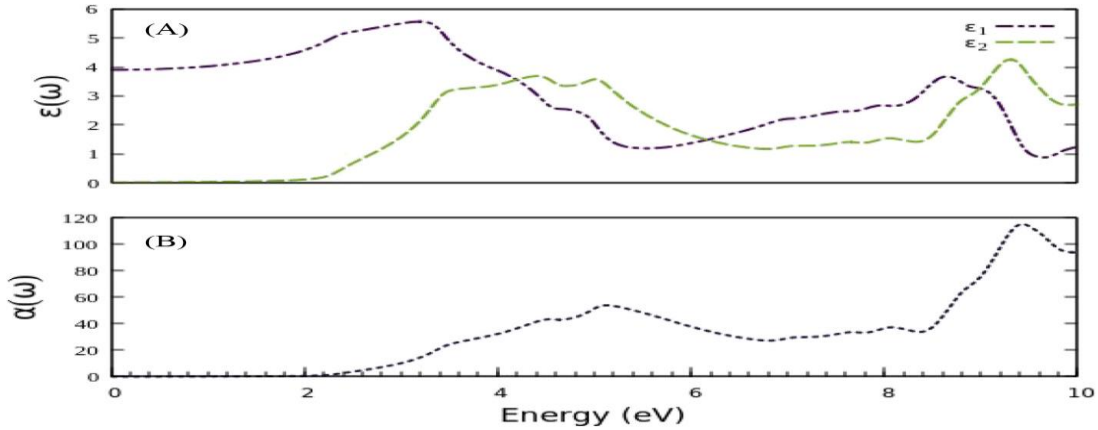

Figure 9: The plotted curve between photon energy in (eV) vs, **(A)** Dielectric parameters $\varepsilon_1(\omega)$ real and $\varepsilon_2(\omega)$ imaginary and **(B)** Absorption coefficient $\alpha(\omega)$ of $CH_3NH_3PbBr_3$ (Choudhary et al. 2020).

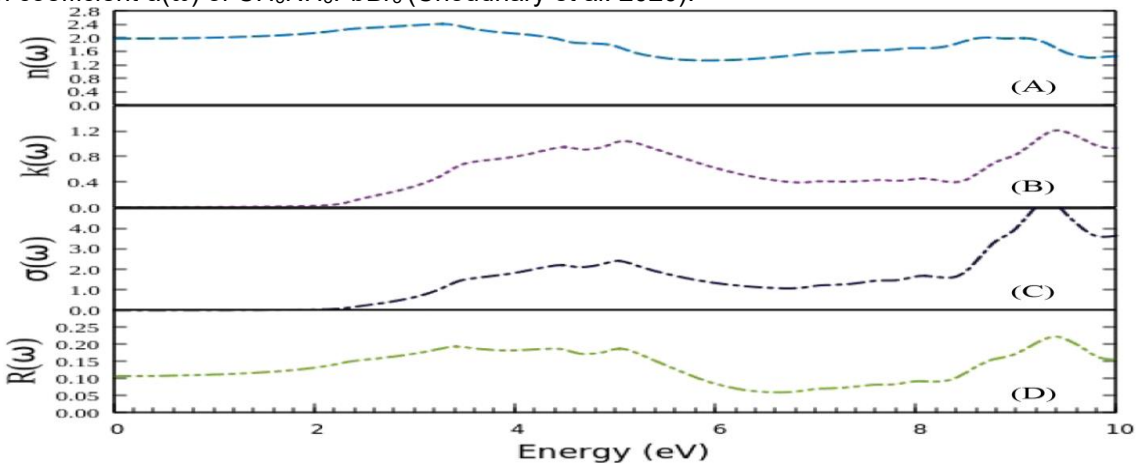

Figure 10: Incident photon energy dependence: (**A)** Refractive index - n(ω), **(B)** Extinction coefficient - k(ω), **(C)**Optical conductivity - σ(ω), and **(D)**Reflection coefficient - R(ω) of $CH_3NH_3PbBr_3$ (Choudhary et al. 2020).

4. CONCLUSION:

In one of the previous studies conducted by the authors, *ab-initio* calculations were conducted for $CH_3NH_3PbBr_3$ to analyse its fundamental properties, focusing on a specific orientation of the organic molecule $CH_3NH_3^+$ in the (111) direction. By modifying the TB-mBJ parameter after the WC-GGA approximation, a band gap of 2.27 eV was determined, indicating it as a direct band gap semiconductor. The absorptive spectra of the dielectric function revealed major peaks attributed to electron transitions from Pb s and p states, with significant contribution from Br p states to unoccupied Pb p orbitals. Despite its promising optical properties for optoelectronic devices, the toxic and unstable nature of lead-based perovskites highlights the need for more stable and environmentally friendly alternatives.

In contrast, $Cs_2AgBiBr_6$, a lead-free halide double perovskite, was studied for its structural, electronic, and optical properties using density functional theory. The material exhibited an indirect band gap of 1.8 eV, making it a potential replacement for lead-based perovskites. Examination of optical characteristics including dielectric function, reflectivity, absorption coefficient, optical conductivity, refractive index, extinction coefficient, and energy loss demonstrated the potential of $Cs_2AgBiBr_6$ for use in lead-free and non-toxic optoelectronic devices. The research underscores the importance of conducting additional experimental inquiries into the electronic and optical attributes of lead-free halide double perovskites to further elucidate their properties and potential applications.

REFERENCES:

Bartel, C. J., Sutton, C., Goldsmith, B. R., Ouyang, R., Musgrave, C. B., Ghiringhelli, L. M., & Scheffler, M. (2019). New tolerance factor to predict the stability of perovskite oxides and halides. *Science advances*, *5*(2), eaav0693.

Birch, F. (1947). Finite elastic strain of cubic crystals. *Physical review*, *71*(11), 809.

Cheng, J., & Yang, Z. Q. (2006). Electronic structures of double perovskites Ba2MnMO6 (M= W and Re) from first-principles studies. *physica status solidi (b)*, *243*(6), 1151-1158.

Choudhary, S., Shukla, A., Chaudhary, J., & Verma, A. S. (2020). Extensive investigation of structural, electronic, optical, and thermoelectric properties of hybrid perovskite (CH3NH3PbBr3) with mechanical stability constants. *International Journal of Energy Research*, *44*(14), 11614-11628.

Eames, C., Frost, J. M., Barnes, P. R., O'regan, B. C., Walsh, A., & Islam, M. S. (2015). Ionic transport in hybrid lead iodide perovskite solar cells. *Nature communications*, *6*(1), 1-8.

Ece Eyi, E., &Cabuk, S. (2010). Ab initio study of the structural, electronic and optical properties of NaTaO3. *Philosophical Magazine*, *90*(21), 2965-2976.

Giustino, F., & Snaith, H. J. (2016). Toward lead-free perovskite solar cells. *ACS Energy Letters*, *1*(6), 1233-1240.

Green, M. A., Ho-Baillie, A., & Snaith, H. J. (2014). The emergence of perovskite solar cells. *Nature photonics*, *8*(7), 506-514.

Hohenberg, P., & Kohn, W. (1964). Inhomogeneous electron gas. *Physical review*, *136*(3B), B864.

Johnsson, M., & Lemmens, P. (2005). Crystallography and chemistry of perovskites. *arXiv preprint cond-mat/0506606*.

Jung, H. S., & Park, N. G. (2015). Perovskite solar cells: from materials to devices. *small*, *11*(1), 10-25.

Kohn, W., & Sham, L. J. (1965). Self-consistent equations including exchange and correlation effects. *Physical review*, *140*(4A), A1133.

Li, J., & Rinke, P. (2016). Atomic structure of metal-halide perovskites from first principles: The chicken-and-egg paradox of the organic-inorganic interaction. *Physical Review B*, *94*(4), 045201.

Li, Z., Yang, M., Park, J. S., Wei, S. H., Berry, J. J., & Zhu, K. (2016). Stabilizing perovskite structures by tuning tolerance factor: formation of formamidinium and cesium lead iodide solid-state alloys. *Chemistry of Materials*, *28*(1), 284-292.

Luo, S., & Daoud, W. A. (2015). Recent progress in organic–inorganic halide perovskite solar cells: mechanisms and material design. *Journal of Materials Chemistry A*, *3*(17), 8992-9010.

Monkhorst, H. J., & Pack, J. D. (1976). Special points for Brillouin-zone integrations. *Physical review B*, *13*(12), 5188.

Perdew, J. P., Burke, K., &Ernzerhof, M. (1996). Generalized gradient approximation made simple. *Physical review letters*, *77*(18), 3865.

Perdew, J. P., Ruzsinszky, A., Csonka, G. I., Vydrov, O. A., Scuseria, G. E., Constantin, L. A., ... & Burke, K. (2008). Restoring the density-gradient expansion for exchange in solids and surfaces. *Physical review letters*, *100*(13), 136406.

Saha-Dasgupta, T. (2020). Double perovskites with 3d and 4d/5d transition metals: compounds with promises. *Materials Research Express*, *7*(1), 014003.

Shimakawa, Y., Azuma, M., & Ichikawa, N. (2011). Multiferroic compounds with double-perovskite structures. *Materials*, *4*(1), 153-168.

Slavney, A. H., Smaha, R. W., Smith, I. C., Jaffe, A., Umeyama, D., & Karunadasa, H. I. (2017). Chemical approaches to addressing the instability and toxicity of

lead–halide perovskite absorbers. *Inorganic chemistry*, *56*(1), 46-55.

Sum, T. C., & Mathews, N. (2014). Advancements in perovskite solar cells: photophysics behind the photovoltaics. *Energy & Environmental Science*, *7*(8), 2518-2534.

Tran, F. (2018). WIEN2k: An Augmented Plane Wave Plus Local Orbitals Program for Calculating Crystal Properties.

Vargas, B., Rodríguez-López, G., & Solis-Ibarra, D. (2020). The emergence of halide layered double perovskites. *ACS Energy Letters*, *5*(11), 3591-3608.

Wu, H. (2001). Electronic structure study of double perovskites A 2 FeReO 6 (A= B a, S r, C a) and Sr 2 M MoO 6 (M= C r, M n, F e, C o) by LSDA and LSDA+ U. *Physical Review B*, *64*(12), 125126.

Ziati, M., &Ez-Zahraouy, H. (2021). Theoretical investigation of electronic, optical and thermoelectric properties of tellurium doped barium titanate (BTO) through modified Becke–Johnson exchange potential. *Optik*, *231*, 166440.